Interpretation of Complex Fatigue Fractures in the Defence Aerospace Industry Using Quantitative Fractography Techniques

Tamara P Chapman, Edward A Saunders
Rolls-Royce plc., Failure Investigation, Defence Aerospace Operations Facility, Bristol, BS34 7QE
UNITED KINGDOM

Tamara.Chapman3@Rolls-Royce.com, Edward.Saunders@Rolls-Royce.com

Keywords: Damage Propagation Physics, Quantitative Fractography, Transient High Cycle Fatigue, Propagation Banding, Dynamic Oxidation

ABSTRACT

In the rare event of metallurgical failure in the defence aerospace industry, considerable evidence regarding root cause is captured on the fracture surface. Properly understood, fractographic features can be related to recorded flight data and subsequently to fracture mechanics models. Fractographic techniques such as striation counting are used to observe complex in-service fatigue mechanisms involving combined high cycle and low cycle fatigue failure modes. The intention of this quantitative fractography is to estimate propagation life, understand underlying failure mechanisms and thus support fleet risk mitigation management through defined inspection intervals. As discussed in two case studies, examination of in-service compressor and turbine blade fracture surfaces revealed a complex network of macro and micro-scale fatigue propagation banding, generated by intermittent crack progression and arrests/pauses. The ratios between various levels of macro and micro-scale bands were established by quantitative fractography. With reference to recorded flight data these ratios were correlated to the ratios between flights and engine throttle movements that triggered significant vibration transients. Further, through the combination of low and high cycle fatigue loadings, stress and fracture mechanics models were able to correlate predicted crack propagation rates with those estimated via band counting, thus providing mutual validation. Alternating colour changes were also exhibited at a fine band level due to dynamic heating/oxidation from response to different resonant frequencies during fatigue propagation. Identification of the resonant frequency that leads to critical crack trajectory can therefore provide crucial evidence towards root cause understanding and subsequently benefit future blade design.

1.0 INTRODUCTION

In industry it has been estimated that 80-90% of mechanical failures are due to metallurgical fatigue propagation [*Bhaduri, 2018*], [*Findlay, Harrison, 2002*]. It is therefore imperative that in-service fatigue cracking, and the impact on component life, is well understood. In practice, a combination of meticulous analyses through forensic-type failure investigation, stress analysis and fracture mechanics are employed to glean this understanding. The present paper will focus on the use of applied quantitative fractography techniques in the context of two recent failure investigations, where we were able to link the forensic analysis to aircraft flight data and fracture mechanics.

In the rare case of high impact critical failures in the defence aerospace industry, the ability to differentiate between a fatigue fracture that has developed via Low Cycle Fatigue (LCF), High Cycle Fatigue (HCF) or a combination of the two is crucial for effective fleet management. However, such differentiation between LCF and HCF failures is classically very difficult, often made more challenging by a lack of surrounding information; the failure investigator is often forced to rely solely upon the evidence presented by the fracture surface. Accurate determination of the specific fatigue mechanism enables fundamentally different field

mitigation strategies to be employed in order to maintain aircraft fleet readiness.

LCF is commonly attributed to low frequency load application (low number of cycles to failure), generally applied under high stress levels [*Pineau, 2013*], [*Suresh, 1998*]. The plastic strain amplitude is the key fatigue life-controlling parameter, which is itself controlled by fatigue ductility [*Coffin, 1954*], [*Manson, 1954*]. This is given by equation (1), where ε_{pl} is the plastic strain, ε'_f is the fatigue ductility coefficient, N_f is the number of cycles to failure and c is the fatigue ductility exponent [*Mughrabi, 2013*], [*Mughrabi, 2015*]:

$$\frac{\varepsilon_{pl}}{2} = \varepsilon'_f (2N_f)^c \quad (1)$$

When the elastic strain amplitude component begins to exceed the plastic strain amplitude component, the fatigue strength (or fatigue limit) becomes the governing factor in the fatigue life [*Mughrabi, 2013*]. For a number of materials, this transition occurs at a propagation life in the order of ~10^5 cycles, and has been classified as the definition of a transition to a HCF mechanism [*Mughrabi, 2013*]; this may be observed by the flattening of the Wöhler stress versus number of cycles to failure (S-N) curve (Figure 1) [*Wöhler, 1870*]. HCF failures are commonly attributed to high frequency load applications (high number of cycles to failure) but applied under low stress levels.

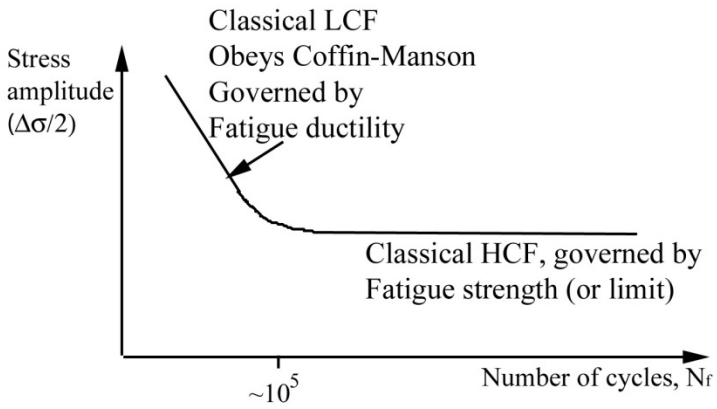

Figure 1: Example of Wöhler (S-N) curve

In the aerospace industry, LCF loadings are usually attributed to engine cycles, i.e. flights, and minor cycles to significant throttle movements or other low frequency applied loadings, e.g. pressure cycles. Conversely, HCF loadings are commonly accredited to vibrational cycles that would arise from component resonances or flutter conditions triggered at certain engine speeds. In military applications, flight profiles can be very complex and vary significantly between different mission and sortie types (Figure 2). In such circumstances, flights, engine throttles and vibrational loading can all be invoked during the propagation of a fatigue crack system. This kind of combined cycle fatigue crack growth can be defined as “complex fatigue” or “combined cycle fatigue” but within Rolls-Royce it is referred to as “transient HCF” in order to clearly differentiate it from sustained HCF loading. Transient HCF implies an intermittent HCF mode, i.e. the passage through short term vibration transients (on/off resonance), which is superimposed on an underlying LCF stress cycle.

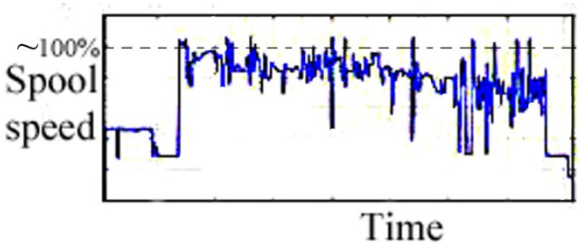

Figure 2: Example military engine flight sortie (*not a real case*)

The utilisation of developing technologies will soon provide great benefit to understanding these complex failures, but in the meantime investigators resort to quantitative fractography techniques, which have seen notable development in recent years [*DeVries, Ruth, Dennies, 2010*], [*Wanhill, Barter, Molent, 2019*], [*Barter, Molent, Wanhill, 2009*], [*Milella, 2013*], [*Wanhill, Hattenberg 2018*], [*Wulpi, 2013*], [*Lynch, 2007*], [*Lynch, 2017*]. Such techniques enable estimation of propagation lives, which is key with regards to mitigation of in-service issues through well-placed inspection intervals [*Gomes, Wellison, Beck, 2014*]. Striation counting is one such technique that has been well known for decades [*DeVries, Ruth, Dennies, 2010*], [*Wulpi, 2013*], [*Connors, 1994*], and tends to be employed for cracks governed largely by striated growth resulting from LCF propagation. Many organisations have written procedures in place but this practice is limited by a number of validity issues, such as a 1:1 ratio between striation formation and loading cycles. In reality it can take hundreds or even thousands of applied cycles before a single striation forms [*Ritchie et al, 1999*], [*Bulloch, Callagy, 2010*], [*Broek, 1974*], [*Plumbridge, 1978*], [*Bathias, Pelloux, 1973*], [*Bates, Clark, 1969*], [*Heiser, Hertzberg, 1971*], [*Hertzberg, Paris, 1965*], [*Kershaw, Liu, 1971*], [*Miller, 1969*], [*Pineau, Pelloux, 1974*], [*Yokobori, Sato, 1976*]. This is particularly notable at low stress-intensity ranges (ΔK) where true propagation is occurring at crack depths below where the Paris-Ergodan law holds true, i.e. stage 1 or structure-sensitive fatigue region [*Paris, Erdogan, 1963*]. The situation improves toward a 1:1 ratio as ΔK rises, thus striation counting may still be employed in circumstances where the validity issues are well understood [*Lynch, 2017*], [*Wanhill, Hattenberg 2018*].

When complex fatigue crack systems have been active, the fracture surface is observed to be covered with an array of fatigue bands, commonly referred to as beach marks, conchoidal markings, clam shell marks, etc. This banding, often irregular in individual spacings, will be seen as coarse to fine and observed by naked eye, optical microscopy and under a Scanning Electron Microscope (SEM) up to very high magnifications. Each observed band usually corresponds to a group (or event) containing multiple numbers of applied cycles, as opposed to single load cycles where genuine fatigue striations are observed [*Pilchak et al., 2009*], [*Lynch, 2007*], [*Wanhill, Barter, Molent, 2019*], [*Barter, Molent, Wanhill, 2009*]. Fatigue bands resulting from complex fatigue propagation (or transient HCF) can be distinguished in their appearance from fatigue striations. They are often more brittle or flat in appearance with thin boundaries/edges and appear at a range of different magnifications. Conversely, genuine fatigue striations convey a greater sense of plasticity in their form as they are formed via a slip process and plastic blunting at the crack tip [*Laird, 1967*], appearing wave-like, saw-tooth or sinusoidal. Striations are also usually more regular in appearance, most often appearing with spacings in a 10^{-4} to 10^{-3} mm order of magnitude, and are thus observed over narrower magnification ranges.

Attempts to estimate crack propagation of complex fatigue systems using quantitative fractography have classically been avoided due to a high degree of uncertainty brought about by the complex nature of the resulting fracture surfaces. However, in some critical failures attempts have been made to estimate the ratios between different levels of banding observed at particular set magnification ranges [*Barter, Molent, Wanhill, 2009*], [*Wulpi, 2013*]. These ratios can then be compared against recorded engine data that may relate to ratios between certain engine and component loading events. Additionally, such work can be supported via estimation of total band quantities at a number of different levels and comparing those against propagation rates estimated through stress and fracture mechanics calculations from combined LCF and HCF loadings

[*McEvily, Ishihara, Mutoh, 2019*].

In this paper we give two examples of these techniques, known as “band counting” or “band matching”. Both have enabled estimations of growth rate and have proven useful for in-service mitigations and fleet management through careful employment of non-destructive examination techniques at set service duration intervals. Crack propagation rates from band counting were also subsequently verified by supporting oxygen profiling analyses across the fracture surfaces.

2.0 QUANTITATIVE FRACTOGRAPHY TECHNIQUES

2.1 Band Counting

The typical feature of a transient HCF fracture surface is the depiction of an array of macro and micro banding on the fracture surface at various levels that act as event markers, e.g. Level 1 (L1), Level 2 (L2), Level 3 (L3), etc. One band level is suggested to be related to flights and higher or coarser levels could show distinctions between different days of flying. Further, lower or finer levels of banding could show throttle movements where passages through active resonance occur, or even individual vibrational frequency perturbations. This fatigue banding is commonly referred to in literature as beach marks, conchoidal markings, clam shell marks, etc.

Band counting involves measuring a series of band widths at different levels to generate average band spacings at each level. Band ratios between different levels are then calculated and compared to typical flight data. It must be emphasised that due to the nature of the band counting technique, it is inherently subjective and numbers extracted from results should be treated with appropriate caution. During a band counting exercise only a proportion of the total bands on the fracture surface are measured.

2.2 Band Matching

Band matching differs from band counting inasmuch as it involves the direct measurement of individual band widths across a fracture surface. Band matching can be employed when two or more different fractography types are observed at the same band level. Fractography types may be differentiated by a number of features, such as observed colour under visual light, the directions of ratchet lines or delineations observed under electron optics and in some cases the crack trajectory, i.e. the direction of crack growth with respect to the principle loading axis. During a band matching exercise the widths of all bands from a given level are measured and recorded against their specific type, with the aim of comparing this against actual time on condition transients (even durations) from flight data. Depending on the feature by which the band type is differentiated, band matching may be limited to coarser band levels only, i.e. if differentiated by colour the band types must be resolvable by optical microscopy alone.

2.3 Oxygen Profiling

Chemical analysis on the fracture surfaces was conducted by semi-quantitative Energy Dispersive X-ray (EDX) analysis in the Scanning Electron Microscope (SEM). Composition profiles produced using simple line scan functions typically generate data that is highly scattered and therefore can conceal subtle trends. In this case area spectra (~80 × 80 μm) at set accelerating voltages were instead taken at recorded depths across the fracture surface from the origins to the crack tip. This enabled a logarithmic plot of oxygen content vs distance from the crack tip to be generated, which could be interrogated to understand the evolution of the oxide layer with time. Attempts were also made to correlate oxygen content to different band types differentiated by alternating colour changes on the fracture surface.

3.0 CASE STUDIES

3.1 Case Study 1 – Turbine Blade Release

3.1.1 Overview of Failures

In recent years there were three similar significant events involving the same military aircraft from two different operators. The events were ultimately shown to have resulted from a single turbine blade release in each case. These turbine blades had a root with a firtree form and were manufactured from a single crystal nickel alloy, SRR99. In all cases the blades had failed between the two outermost serrations, below the platform. Fracture of the released blades was due to fatigue development, specifically via a transient HCF mechanism. A characteristic array of macro and micro banding was therefore observed on the fracture surfaces (Figure 3).

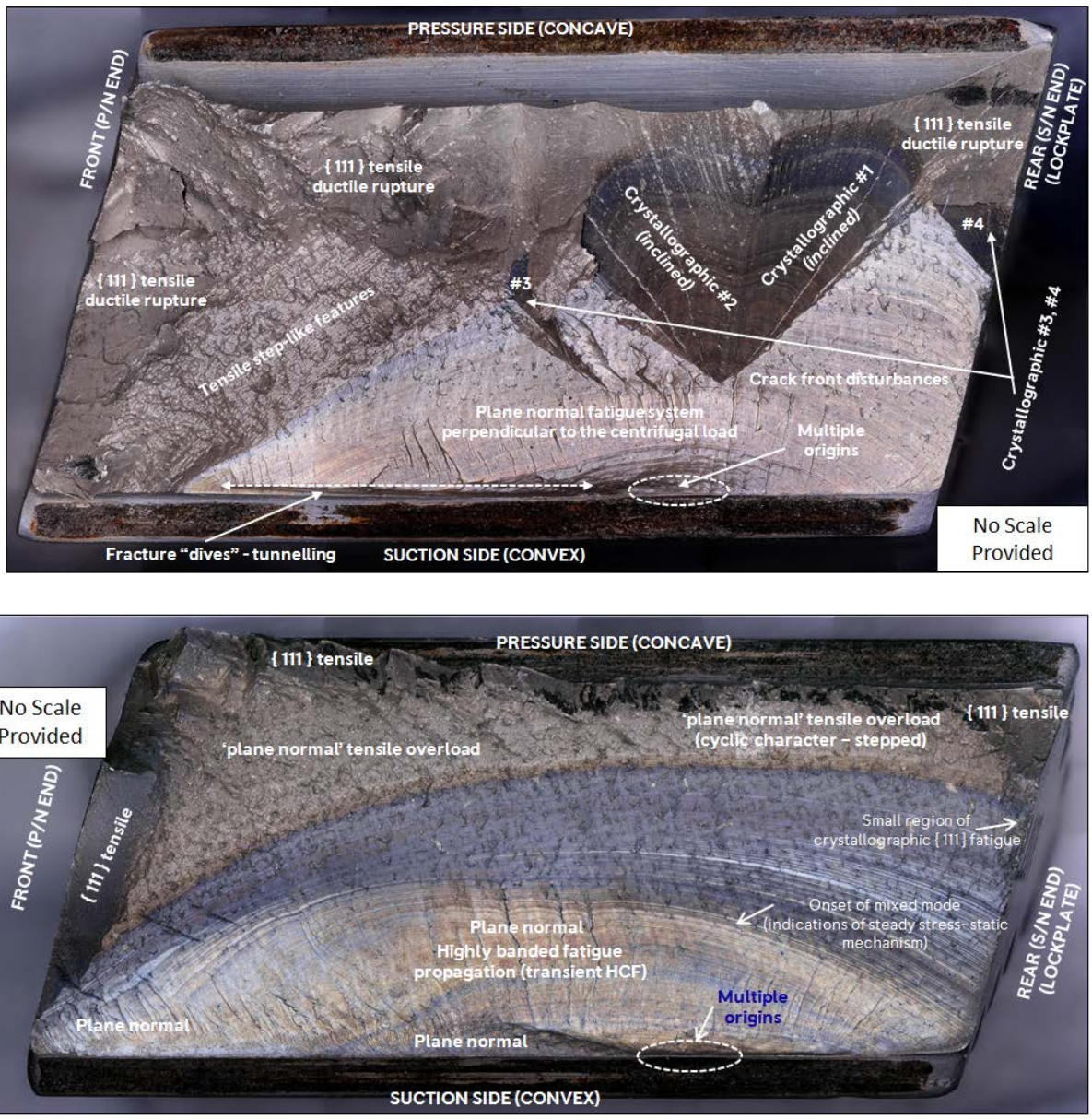

Figure 3 – Two examples showing the colour banding on the released blade fracture surfaces

The fatigue cracks had propagated via passage through certain engine speeds at which particular vibration modes were excited. Although the LCF contribution provided a significant proportion of the overall stress intensity range (ΔK), it was the HCF stress intensity range (ΔK_{HCF}) that was driving crack growth by local progression at the crack tip by providing an increase to the 0-K_{max} cycle to drive the crack forward.

In all three cases the macroscopic crack trajectory of the primary failed blades was across the blade root to failure, i.e. perpendicular to the blades' principle stress axis. In each event, several other blades were also observed to contain one or more cracks in the firtree serrations. However, in the vast majority of cases the macroscopic crack trajectory of theses cracked blades was inboard down through the serration lobe, i.e. approximately parallel to the principle stress axis (and opposite to the centrifugal load). Even if these cracks had grown to failure only minor material loss to serration tips would have occurred. Microscopically, the released blade fracture surfaces showed evidence of an alternating crack trajectory. The crack trajectory was observed to alternate in a step-like manner between perpendicular and parallel to the principle stress axis of the blade (Figure 4).

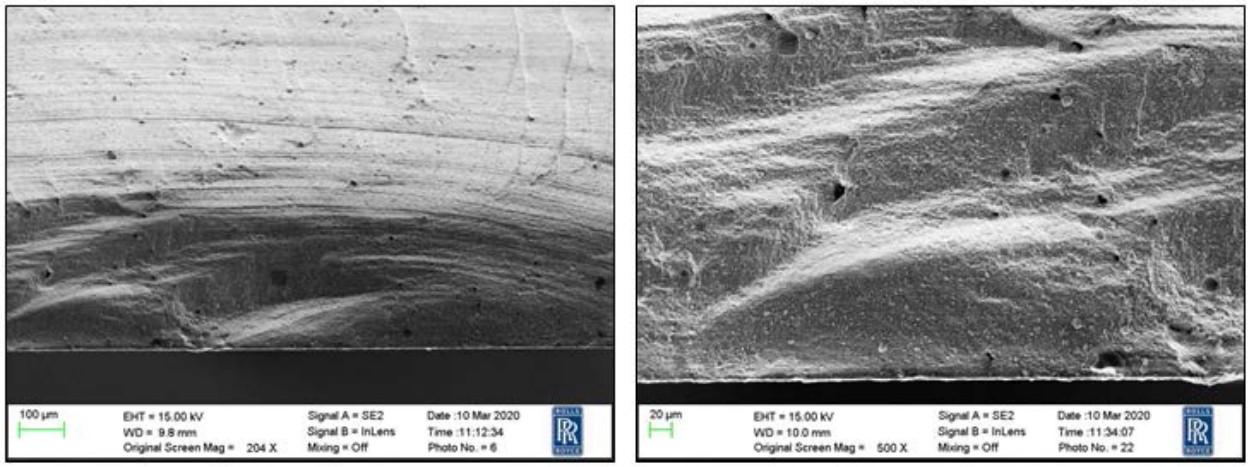

Figure 4 – Crack trajectory alternating in a step-like manner

Two different fractography types were also observed on the fracture surface. It was proposed that these could relate to two main dynamic resonant vibration modes that drove the crack in transient HCF. The different bands were therefore also associated with different strain rates and a correspondingly different heat generation, which therefore affected the level of oxidation and oxide thickness. Under optical conditions the individual bands were clearly associated with different colours (arising from variant oxide thickness), which would also be affected by the time spent at underlying ambient temperatures. The different fractography types and colours were also associated with the variant crack trajectories. The two fractography types were denoted as type 1 and type 2 fractography, as follows:

1. Type 1 – generally dark purple/ dark blue in colour1 (optical), lighter delineated appearance (electron): delineations lie ~perpendicular to crack growth direction (Figure 5)

2. Type 2 – generally white/yellow/light blue in colour2 (optical), darker ratchetted appearance (electron): ratchet lines lie in a direction ~parallel to crack growth direction (Figure 5)

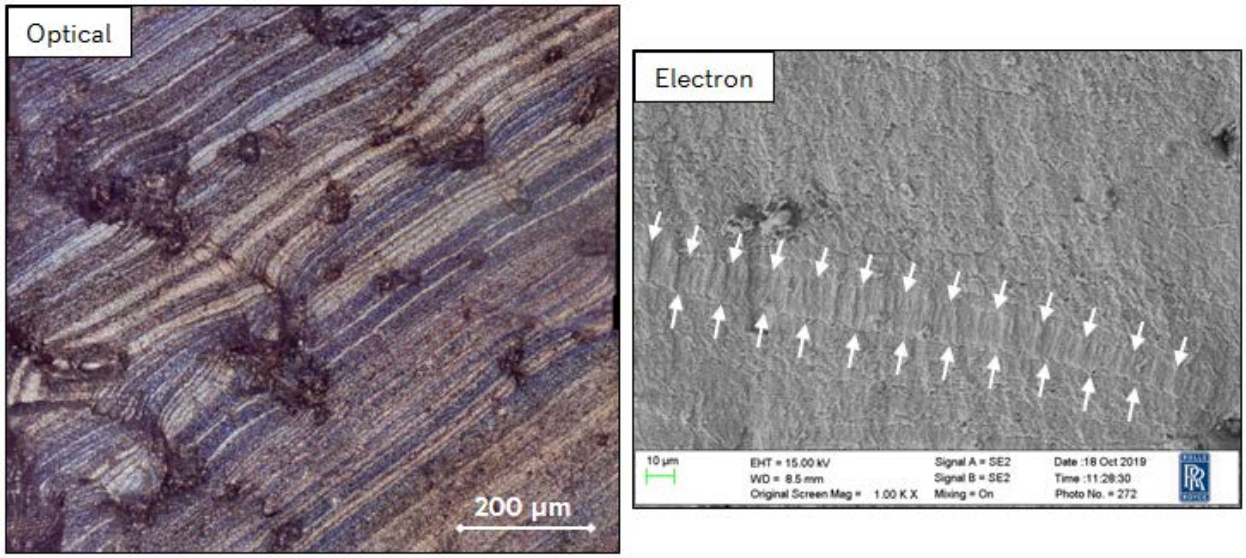

Figure 5 – Type 1 and type 2 fractography

Stress modelling work proposed that three resonant modes were expected to drive transient HCF propagation. These were predicted to occur over certain turbine spool speed (N_L) ranges. It is noted that this speed range alters slightly with different underlying blade crystal orientation, as that influences stiffness (and thus resonant response). Attempts were made to differentiate between these two fractography types and therefore determine if a given engine order mode/frequency was causing the crack to grow perpendicular to the blades' principle stress axis (introducing the possibility of below platform blades release) rather than the less concerning inboard trajectory (down through the serration lobe). Band matching was performed by measuring the physical widths of all resolvable bands across the fracture surface using x1000 optical and secondary electron stitched images; it is recognised that the technique has a measure of human error/subjectivity. Notwithstanding this, the work was undertaken to assess if a correlation existed between time on condition (via scaled band width measurements) at a particular resonance mode, to identify whether an across root crack trajectory could be attributed to a certain engine order. Unfortunately in this case it was not possible to correlate physically measured band widths to time on condition; therefore it was not possible to determine which resonance mode caused the crack to grow perpendicular to the principle stress axis. It is anticipated that the development and introduction of digital imaging recognition software will remove the inherent subjectivity of this technique and may enable resolution of the expected correlations.

Band counting was subsequently performed over a single path from close to the crack origin to the crack tip. It was demonstrated that ~150 level 2 (L2) bands were recorded with an average spacing of ~40 µm and ~875 level 3 (L3) bands were recorded with an approximate spacing of 5-10 µm. The ratio of L3:L2 was therefore ~6 bands. This number was supported by the typical number of throttle movements (minor cycles) through a speed range of ~104% N_L (LP spool speed) over the last 20 flights recorded. It should be noted that 104% N_L is the predicted spool speed range at which the resonant modes driving crack progression occurred. Due to their semi-regular appearance it was postulated that the course level 2 bands may correspond to flights and the finer L3 bands to the number of throttles through a particular resonance or N_L speed. Approximately 150 level 2 bands were recorded across the fracture surface and, noting the typical duration of a flight, it was reasonable to estimate that the age of the crack was in the order of hundreds of hours.

Figure 6 was generated following oxygen profiling across a single crack path on the fracture surface. The oxygen profile showed a fairly consistent plateau region from the origin until ~1mm from the crack tip; average oxygen content in the plateau region was ~15 wt. %. Oxide growth rates are generally logarithmic and will plateau after long durations at temperature, thus the inference of the nominally consistent oxygen

content in a plateau region over the majority of the fracture surface, showed that it had spent a considerable time at the ambient engine running. For instance, it indicated that the crack did not grow so rapidly such that only the early part of the crack was exposed to the environment long enough to develop any significant oxide layer. With reference to (*Hernandez, Saunders and Madariaga, 2018*) it was possible to gauge a rough order of magnitude age for the primary blade crack. It should be noted that the data provided in (*Hernandez, Saunders and Madariaga, 2018*) is for an iron containing nickel alloy, which was exposed as open tensile fracture surfaces to temperatures of 700-750°C and at one atmosphere. At these conditions the logarithmic trend of the data indicated 15 wt. % oxygen would be measured after ~500 hours at temperature. Recognising that the difference in alloy composition and exposure temperature of the gauge data would promote increased oxidation compared with this single crystal turbine blade material at ~550°C, there was considered to be sufficient inference to suggest that the primary failed blade crack had been growing in the order of hundreds of hours. This data therefore further substantiated the band counting findings and also corroborating the idea that the L2 bands were very likely to relate to flights.

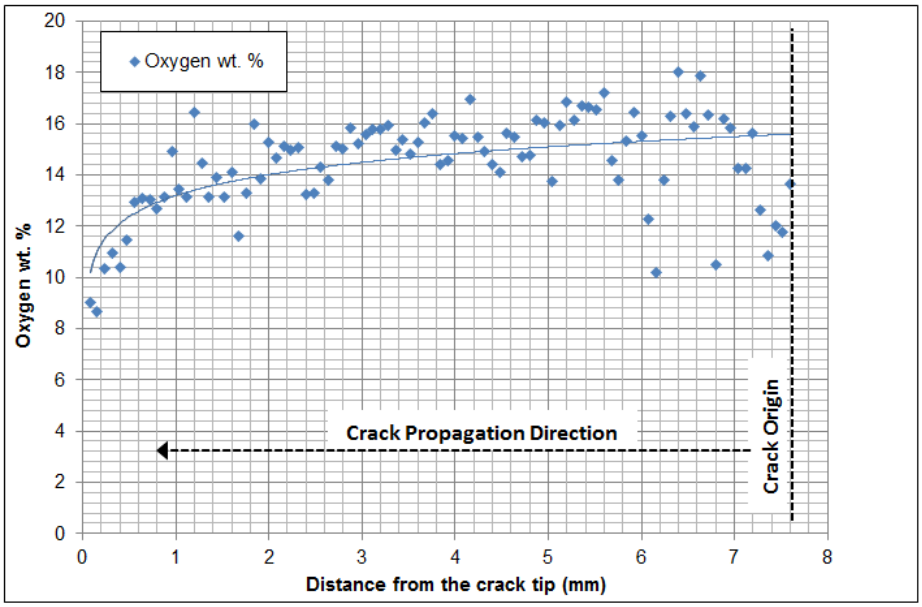

Figure 6 – Oxygen profile demonstrating oxygen content with distance from the crack tip at 15kV

3.2 Case Study 2 – Compressor Blade Release

Recently, there have been two military aircraft accidents that were ultimately shown to have resulted from a compressor blade release, from the same aircraft type. These blades are the kind that include bushed pin hole fixings in the root with two lugs (front and rear), as depicted by the schematic in Figure 7. The blades are fitted to the disc via pins located between the disc and blade fixings. The blade release was due to fatigue development that had initiated from the pinhole bore occurred at the 3-9 o'clock line of the rear lug. The blades were manufactured from aluminium alloy 2618a (RR58).

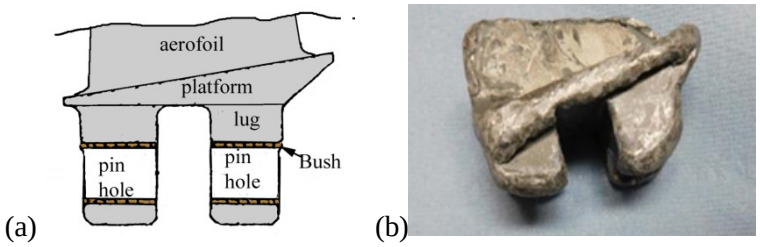

Figure 7 – (a) Schematic representation of the compressor blade root fixing form, not to scale; (b) Shows processed portion of blade root following release *(no scale provided)*

Since these incidents, a few other blades from other engines were identified with cracking at the same location in the rear lug pinhole. These were from the same engine type with two different operators. In each case of blade release and cracking, fatigue initiation had occurred at a position close to the rear lug rear face around the 3 o'clock position (viewed from the rear). One typical opened fatigue crack surface is as shown in Figure 8.

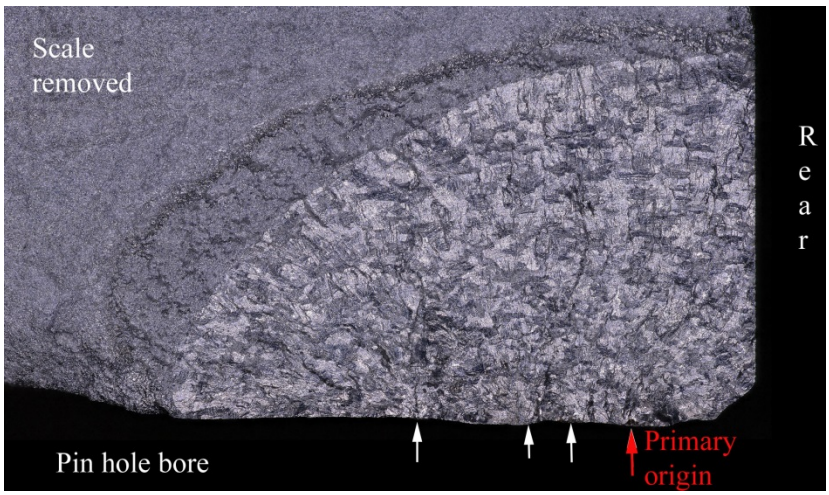

Figure 8 – Showing a typical opened fatigue crack surface. Fatigue origins are arrowed, with the primary in red. The origins are also co-located with dark spots of transferred copper material on the pin hole bore, with migrated copper locally on the open crack surface

A number of metallurgical and stress factors, co-located at the primary origin locations, were assessed to be the underlying cause for fatigue initiation. Metallurgically, these included fretting and metal transfer (copper) between the inserted aluminium bronze bush and pin hole. These appeared as a series of dark spots on the pinhole surface, aligned with original machining lines with higher than drawing tolerance surface roughness (Figure 9). Fretting was consequential of a combination of vibrational resonances and an undersized interference fit between bush and pin, allowing more freedom of movement than normal.

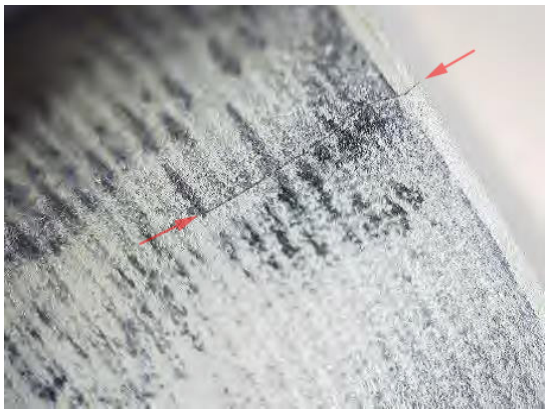

Figure 9 – (a) Showing dark spots from fretting and metal transfer from the bush on the pin hole surface, following bush removal – aligned with original machining lines. The crack is identified between the two red arrows, and runs at the apex of the dark spots. After crack opening, these were shown to be co-incident with fatigue origins

Fatigue initiated at the apex of a number of these spots, which were positions of balancing tensile stress; Figure 10. There was also evidence local overheating and consequent effect to the immediate underlying parent material; Figure 11. The material structure of the blades was otherwise metallurgically satisfactory.

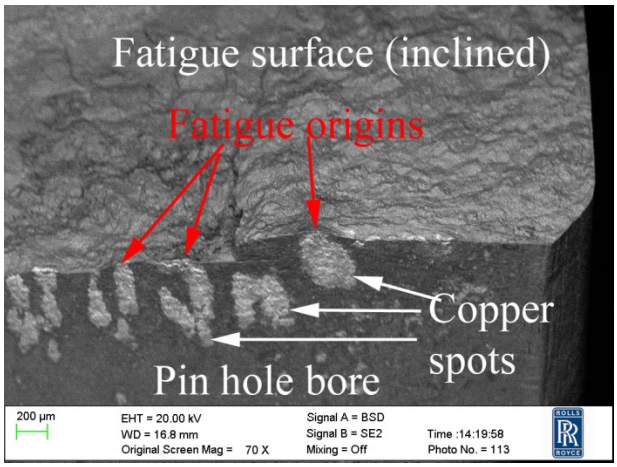

Figure 10 – Backscattered electron image of one of the opened cracks (different from figure 8 and 9) showing fatigue initiation occurring at the apex of transferred copper material from the bush. The image is inclined at ~45° to show both pin hole and open crack surfaces. In electron backscatter imagery the copper appears light against the darker aluminium alloy background.

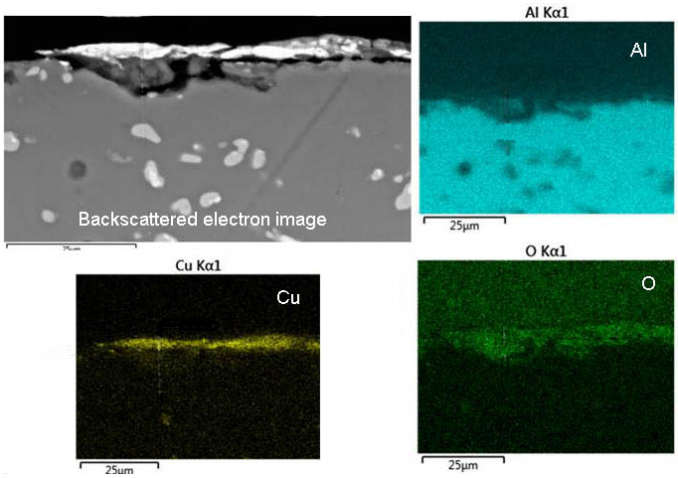

Figure 11 – Section through dark spot at a fatigue origin at the pin hole, observed in backscattered electron and equivalent EDX x-ray maps for aluminium (Al), copper (Cu) and oxygen (O). The copper material transferred from the bush can be seen, and a slight overheated zone beneath (mapped in oxygen), effecting the underlying parent material

Finite element stress analysis, with interrogation of former strain gauge testing, identified a predicted critical location due to a combined peak LCF (worst principal) stress (Figure 12) and peak alternating (vibratory/ resonance) stress. The primary fatigue origins were situated very close to this location. Under certain flight conditions, 2-off chief resonant modes can be excited over a particular, high, compressor spool speed.

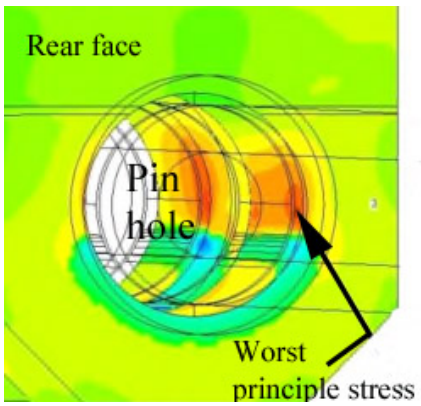

Figure 12 – Showing worst principle stress from finite element model on zoomed in area around pin hole showing peak at ~3 o'clock position (scaling/values removed)

Independent to the stress analysis, fractographic examination showed that fatigue propagation was combined cycle mode. This was predominantly driven by short-term passages through that spool speed exciting resonant conditions to give high cycle growth (HCF) augmented by underlying low cycle flight or throttle-related loadings (LCF/ minor cycles), i.e. transient HCF. There was no evidence of sustained HCF which would occur by operating on resonant modes for prolonged periods.

The fracture surfaces were characterised by banding at three different magnification ranges or levels (L1, L2, L3). Due to variant band width, the fatigue propagates locally at the crack tip under transient HCF, whilst the bands act as event markers indicating the underlying flights, minor LCF cycles and throttle movements. Examples of the banding may be seen in Figure 13 and 14.

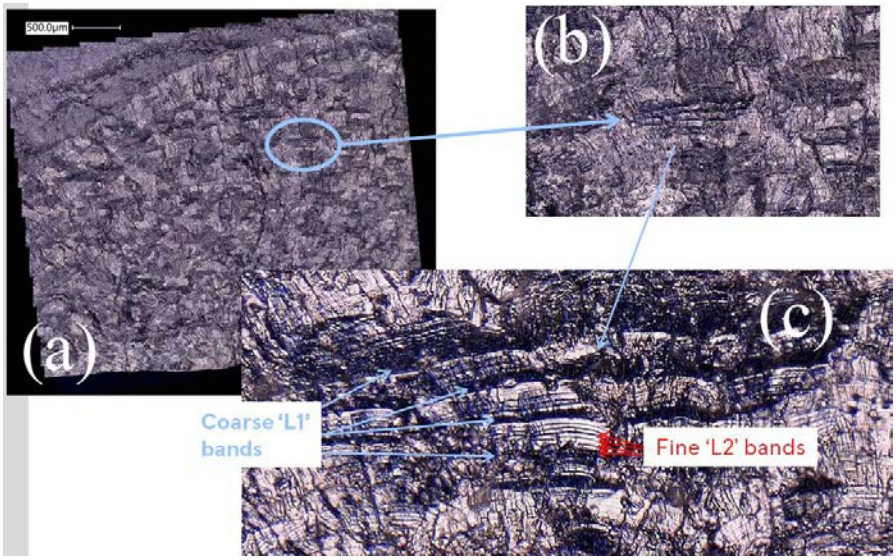

Figure 13 – Optical images of one of the opened fracture surfaces to show the banding observed at an optical level. (a) Shows a segment of an overall opened crack surface where some L1 bands may be seen with close scrutiny (example ringed in blue); (b) Shows the L1 bands more clearly, and (c) shows an example area of L2 bands seen within the L1 bands with increased magnification

Band counting was performed at each of the three different levels. This was done both optically (L1 and L2) and in the SEM (L2 and L3) through assessment of average spacings at a number of crack depths across the full fatigue system surface then integrating to give a total. The typical ratios between those numbers (e.g. number of L2's per L1) were also calculated. Figure 14 shows examples of L2 within L1, and L3 within L2 bands as viewed in electron optics.

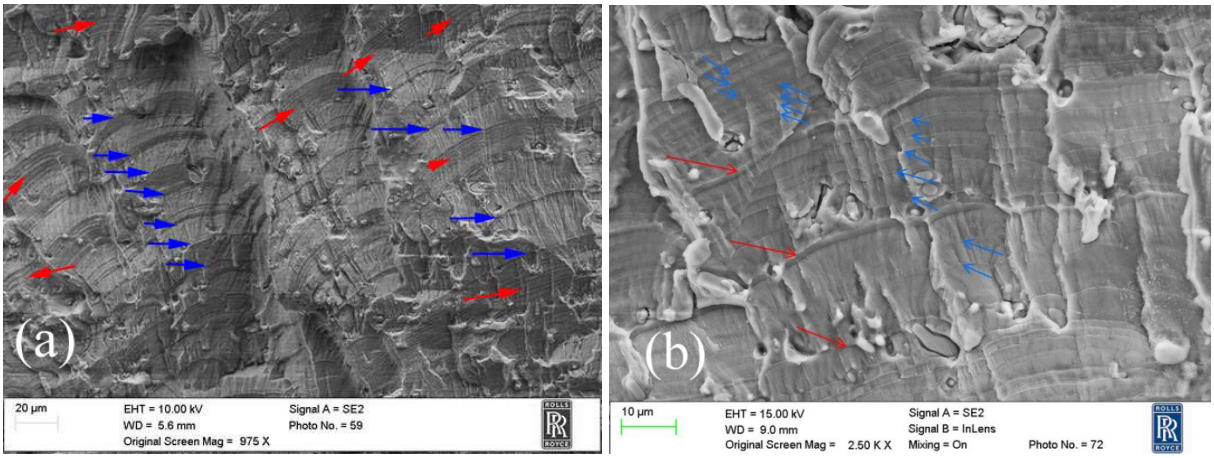

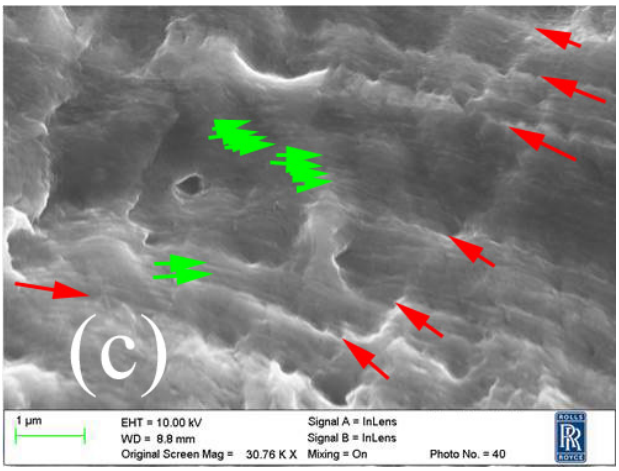

Figure 14 – Secondary electron images of typical examples of the banding: (a) Shows a low magnification image of L1 bands, examples of which are arrowed blue with example groups of L2 bands arrowed red; (b) Example area of L2 bands (arrowed blue) within L1 bands (arrowed red), and (c) higher magnification image of fine L3 bands (examples arrowed green) within L2 bands (arrowed red)

It was found that, for all the cracks studied, there were very similar growth rates in terms of band numbers against crack depths. In all cases hundreds of L1 bands were estimated from a 1.2 mm starting crack depth to overload/ fast fracture of the rear lug. In terms of the bands representing event markers, the L1 bands were proposed to represent flights. This was supported by the fact that they were the coarsest visible bands, their semi-regular nature (on this aircraft, flights are commonly very similar in duration) and the total number was consistent. Interrogation of recorded flight data further supported that proposal.

The number of noteworthy throttles varied considerably each flight. The duration of each crossing through and into the resonant condition was also highly variable. As the L2 bands were irregular in spacing, and the number of L2's per L1 differed for individual circumstances, they were considered to align with significant throttle movements. Flight data for six off typical flights for both operators was examined. Here, the mean number and wide variation of L2's per L1 was compared against the number of crossings through the critical spool speed range that was predicted to excite the resonant condition per flight. From this it was believed that the L2:L1 ratio reflected a representation of numbers of throttles/crossings through the critical speed range.

Fracture mechanics analysis, using only LCF loadings (inclusive of minor cycles), found the predicted growth rate to be much slower than that suggested by the band counting work. However, when HCF cycles were supplemented into the calculations the modelled growth rates were much more comparable. This supported the mechanistic understanding developed from the fractography of a transient HCF/ combined cycle fatigue system where the L1 bands were established as flights. Hence, an estimated crack growth rate for these cracks was obtained, and thereby a suitable inspection interval has been put in place through off-wing and on-wing NDE inspections, which allows the aircraft to operate safely going forward.

4.0 CONCLUSIONS

1. Crack propagation rates have been estimated from the comparison of ratios of average band spacings at different levels against flight data. The resulting data was supported by pertinent fracture mechanics and stress modelling work.

2. Crack propagation rates were further validated by analysis of oxidation trends across crack surfaces

from origin to fracture.

3. Attempts were made to correlate physical widths of all resolvable bands against actual time on condition transients from flight data. It was recognised that the technique in its current form is too prone to subjectivity to identify these subtle trends. However, it is anticipated that the development and introduction of digital imaging recognition software will remove the inherent subjectivity of this technique and may enable resolution of the expected correlations. This in turn may enable identification of particular resonance mode(s) leading to the across root crack trajectories which can lead to below platform blade release.

4. In high profile incident investigations, the investment in performing quantitative fractographic assessments on transient HCF crack systems can result in a reasonable estimation of fatigue crack time and propagation rate. This can in turn support fleet risk management through introduction of defined inspection intervals.

5.0 ACKNOWLEDGEMENT

In gratitude to all those in Rolls-Royce who assisted us in these investigations.

6.0 REFERENCES

[1] Barter, S.A., Molent, L., Wanhill, R.J.H. (2009) “Marker Loads for Quantitative Fractography of Fatigue Cracks in Aerospace Alloys”. In: Bos M.J. (eds) ICAF 2009, Bridging the Gap between Theory and Operational Practice. Springer, Dordrecht. https://doi.org/10.1007/978-90-481-2746-7_2

[2] Bates, R.C. and Clark, W.G. (1969), “Fractography and fracture mechanics,” *Trans. Q. ASM*, 62, No. 2, 380–389.

[3] Bathias, C., Pelloux, R.M. (1973), “Fatigue crack propagation in martensitic and austenitic steels”. *Metall Mater Trans B* 4, 1265–1273 (1973). https://doi.org/10.1007/BF02644521

[4] Bhaduri, A. (2018) “Fatigue”. In: Mechanical Properties and Working of Metals and Alloys. Springer Series in Materials Science, vol 264. Springer, Singapore. https://doi.org/10.1007/978-981-10-7209-3_8

[5] Broek, D. (1974), “Some Contributions of Electron Fractography to the Theory of Fracture”, *International Metallurgical Reviews*, 19:1, 135-182, DOI: 10.1179/imtlr.1974.19.1.135

[6] Bulloch, J.H., Callagy, A.G. (2010), “A detailed study of the relationship between fatigue crack growth rate and striation spacing in a range of low alloy ferritic steels”, *Engineering Failure Analysis* 17 (2010) 168–178

[7] Coffin, LF. (1954), “A study of the effect of cyclic thermal stresses on a ductile metal”. *Trans. Am. Soc. Mech. Eng*. 76, 931–950

[8] Connors, W.C. (1994), “Fatigue striation spacing analysis”, *Mater. Charact*. 33 (3) (October 1994) 245–253

[9] DeVries, P.H., Ruth, K.T. & Dennies, D.P. (2010) “Counting on Fatigue: Striations and Their Measure”. *J Fail. Anal. and Preven.* 10, 120–137 (2010). https://doi.org/10.1007/s11668-009-9320-4

[10] Findlay, S. and Harrison, N., (2002). “Why aircraft fail”. *Materials Today*, 5(11), pp.18-25. DOI: 10.1016/S1369-7021(02)01138-0

[11] Gomes, Wellison and Beck, André. (2014). “Optimal inspection planning and repair under random

crack propagation". *Engineering Structures*. 69. 285–296. 10.1016/j.engstruct.2014.03.021.

[12] Heiser, F.A. and Hertzberg, R.W. (1971), "Anisotropy of fatigue crack propagation," *Trans. ASME, J. Basic Eng*., 93, No. 6, 211-217 (1971).

[13] Hernandez, I., Saunders, E.A., and Madariaga, I. (2018), "Energy Dispersive X-ray technique applied to fatigue fracture surfaces oxidation to provide information on growth rate", *Fatigue 2018*, MATEC Web of Conferences 165, 13006. https://doi.org/10.1051/matecconf/201816513006

[14] Hertzberg, R.W. and Paris, P.C. (1965), "Application of Electron Fractography and Fracture Mechanics to Fatigue Crack Propagation", *Proceedings of the First International Conference on Fracture*, Sendai, Japan (1965), Edition Yokobori, Kawasaki and Swedlow, p. 459

[15] Kershaw, J. and Liu, H.W. (1971), "Electron Fractography and Fatigue Crack Propagation in 70075-T6 Aluminium Sheet", *International Journal of Fracture Mechanics*, Vol. 7, 1971.

[16] Laird, C. (1967), "The Influence of Metallurgical Structure on the Mechanisms of Fatigue Crack Propagation", ASTM STP 415, *Am. Soc. Testing Mats.*, P. 131

[17] Lynch, S.P. (2007), "Progression markings, striations, and crack-arrest markings on fracture surfaces", *Materials Science and Engineering A* 468–470 (2007) 74–80

[18] Lynch, S.P. (2017), "Some fractographic contributions to understanding fatigue crack growth", *International Journal of Fatigue*, Volume 104, November 2017, Pages 12-26

[19] Manson, S.S. (1954), "Behaviour of materials under conditions of thermal stress". In National advisory board commission on aeronautics: report 110. Cleveland, OH: Lewis Flight Propulsion Laboratory

[20] McEvily, A.J., Ishihara, S., and Mutoh, Y. (2015), "1989 DC-10 crash: A cold case mystery solved", *Engineering Fracture Mechanics* 157 (2016) 154–165

[21] Milella, P.P. (2013), "Morphological Aspects of Fatigue Crack Formation and Growth (Chapter 2)", Fatigue and Corrosion in Metals, Springer-Verlag Mailand, pages 73-108

[22] Miller, G.A. (1969), "Fatigue fracture appearance and kinetic of striation formation in some high-strength steels," *Trans. Q. ASM*, 62, No. 6, 651–658

[23] Mughrabi, H. (2013), "Microstructural fatigue mechanisms: Cyclic slip irreversibility, crack initiation, non-linear elastic damage analysis", *International Journal of Fatigue, Volume 57*, December 2013, Pages 2-8. https://doi.org/10.1016/j.ijfatigue.2012.06.007

[24] Mughrabi, H. (2015). "Microstructural Mechanisms of Cyclic Deformation, fatigue Crack Initiation and Early Crack Growth". *Philosophical Transactions of the Royal Society A*, 373, pp 1-21, The Royal Society, London. https://doi.org/10.1098/rsta.2014.0132

[25] Paris, P.C. and Erdogan, F. (1963) "A Critical Analysis of Crack Propagation Laws". *Journal of Basic Engineering*, 85, 528-533. http://dx.doi.org/10.1115/1.3656900

[26] Pilchak, A.L., Bhattacharjee, A., Rosenberger, A.H., Williams, J.C. (2009), "Low DK faceted crack growth in titanium alloys", International Journal of Fatigue 31 (2009) 989–994

[27] Pineau, A.G., Pelloux, R.M. (1974) Influence of strain-induced martensitic transformations on fatigue crack growth rates in stainless steels. *Metall Mater Trans B* 5, 1103–1112 (1974). https://doi.org/10.1007/BF02644322

[28] Pineau, A. *(2013), "Low-Cycle Fatigue", Fatigue of Materials and Structures: Fundamentals: 113–177*

[29] Plumbridge, W.J. (1978). "Problems associated with early stage fatigue crack growth". *Metal Science*. 12. 251-256.

[30] Ritchie, R.O., Davidson, D.L., Boyce, B.L., Campbell, J.P. And Roder, O. (1999), “High cycle fatigue of Ti–6Al–4V”, Blackwell Science Ltd. *Fatigue Fract Engng Mater Struct* 22, 621–631

[31] Suresh, S. (1998), “Fatigue of Materials, Second edition”, Cambridge University Press, Cambridge, UK

[32] Wanhill, R.J.H. and Hattenberg, T. (2018), “Fractography-Based Estimation of Fatigue Crack "Initiation" and Growth Lives in Aircraft Components”, Structural Integrity and Failure (SIF 2006), Sydney, Australia

[33] Wanhill, R.J.H., Barter, S., Molent, L. (2019), “Fatigue Crack Growth Failure and Lifing Analyses for Metallic Aircraft Structures and Components”, Springer Netherlands. DOI: 10.1007/978-94-024-1675-6

[34] Wöhler, M. (1870), Über die Festigkeitsversuche mit Eisen und Stahl. Z. Bauwesen 20, 73–1, Ernst & Korn

[35] Wulpi, D.J. (2013), Understanding How Components Fail, 3rd Edition, editor Brett Miller, ASM International, Materials Park, Ohio, USA

[36] Yokobori, T. and Sato, K. (1976), “The effect of frequency on fatigue crack propagation rate and striation spacing in 2024-T3 aluminum alloy and SM-50 steel,” *Eng. Fract. Mech.*, 8, No. 1, 81–88 (1976).